Nonlinear Dyn
DOI 10.1007/s11071-012-0392-4

ORIGINAL PAPER

Active flutter suppression control law design method based on balanced proper orthogonal decomposition reduced order model

Chen Gang · Sun Jian · Li Yueming

Received: 5 October 2011 / Accepted: 6 March 2012

Abstract Active control for nonlinear aeroelastic structures is an attractive innovative technology. The design of classic active flutter controllers has often been based on low-fidelity and low-accuracy linear aerodynamic models. Multi-physics high-fidelity reduced order model (ROM) was used to design active control laws. In order to provide a lower-order model for controllers design, a balanced proper orthogonal decomposition ROM (POD-BT/ROM) was investigated. A state-space aeroservoelastic model and the active flutter suppression control law design method based on POD-BT/ROM were proposed. The effectiveness of the proposed method was then demonstrated by NACA 0012 airfoil, AGARD 445.6 wing and the Goland wing+ aeroelastic model.

Keywords Reduced order model · Proper orthogonal decomposition · Balanced truncation · Flutter suppression · Optimal static output feedback

1 Introduction

Flutter is a dynamic instability caused by the interaction of aerodynamic, elastic and inertial forces. It can lead to the sudden mechanical failure of an aircraft wing during fight. The active control of nonlinear aeroelastic instability, such as active flutter suppression, is becoming a promising and attractive technology, because it can simultaneously reduce the weight and increase the performance of modern aircrafts [1]. Many kinds of classic and modern control theories have been applied to design active control laws, such as linear quadratic regulator (LQR), linear quadratic Gaussian (LQG) and robust H_∞ controllers [1–3]. In order to account for the nonlinear effects, gain-scheduled linear parameter-varying (LPV) controllers are also applied to suppress flutter where the model varies smoothly as a function of the selected scheduling parameters [4–6].

The design of classic active flutter controllers are usually based on low-fidelity linear aerodynamic model, such as Theodorsen quasi-steady aerodynamic model [4], the lift surface theory, and the doublet-lattice method [7]. These low-fidelity models have led to great achievements in the design of classic flutter controllers, especially in the low-speed subsonic regime. However, these methods require good prior knowledge and experience regarding the characteristics of the aeroelastic system. The generalized unsteady aerodynamic forces must be calculated for each structural mode over a wide range of frequencies. And then, they must be transformed into the time domain to construct the aeroservoelastic model by the rational function approximation [7, 8], which is a tedious process. The greatest shortcoming of this approach is that

C. Gang · S. Jian (✉) · L. Yueming
State Key Laboratory for Strength and Vibration of Mechanical Structures, School of Aerospace, Xi'an Jiaotong University, Xi'an 710049, China
e-mail: sunjian10@mail.xjtu.edu.cn

Published online: 16 June 2012

the low-fidelity linear aerodynamic model cannot accurately capture the dominant nonlinear unsteady behaviors of the transonic flow, such as shock movement and flow separation, which have significant impacts on the aeroelastic responses.

As a benefit of the development of computational aeroelasticity, the nonlinear aeroelastic response can be accurately predicted by the physics-based high-fidelity CFD/CSD coupled solver. However, the use of multi-step time domain calculations for each aircraft state is computationally expensive. The high dimensionality of the full-order CFD model also prevents its application to controller design. To reduce the expensive computational cost and the high order of the CFD model, a novel concept, called the reduced-order model, has been proposed in recent years. The ROM seeks to capture the dominant nonlinear behaviors of the aeroelastic system with the use of a simple mathematical representative model constructed from the full-order system. The use of this model is convenient in conceptual design, control and data-driven systems [9–11]. Different approaches for reduced-order modeling of aerodynamic systems have been proposed, including system identification-based data-driven model, such as Volterra theory of nonlinear systems [8] and linear model fitting ARMA model [12], as well as flow eigenmode-based models, such as harmonic balance (HB) method, proper orthogonal decomposition (POD) method [13, 14], and the nonlinear dynamic theory based models [15, 16].

Recently the proper orthogonal decomposition based reduced order model (POD/ROM)becomes one of the most popular ROM methods for aeroelastic system. POD method was firstly used by Romannowski to construct ROMs for a two-dimensional airfoil aeroelastic system in transonic flow [17]. POD/ROM has been widely used in linear and nonlinear aeroelastic analysis [18–26]. There are two types of POD/ROM construction methods, including the time-domain method and the frequency-domain method. In the frequency domain, a small scale snapshots matrix around the characteristic frequency is good enough to capture the dominate behavior of the flow. So that the frequency-domain method can lead to lower order ROMs [9–11]. The time-domain POD/ROM requires a full frequency spectral input signal to construct the snapshots matrix. Usually the order of the time snapshots matrix is larger than the frequency's, which leads to a higher order ROM. For example, a 55-order HB/ROM can obtain enough accurate prediction results for Agard wing [19], however, 300-order model is required for the time-domain POD/ROM to obtain the same accuracy [27]. On the other hand, the larger time snapshot matrix includes much more information of the original aeroelastic system, which is helpful to increase the robustness of ROMs [23, 28]. The robustness of models is very important for active controller design and flight dynamics modeling That's why the time-domain POD/ROM is also widely used in aeroelastic simulation [29, 30], especially in the coupled problems with flight dynamics [28, 31–33].

Low order and robust models would be better for control law design. The system identification based ROM such as Volterra/ROM has been applied to design active flutter suppression controllers for airfoil [34], BACT wing model [35], and Goland+ wing [36]. However, as one of the most popular and promising ROMs, POD/ROM is still seldom applied in flutter suppression. In this study, we will develop an active control law design method based on the time-domain POD/ROM. In order to overcome the shortcoming of the traditional time-domain POD/ROM, by introducing the balanced truncation algorithm [37], a lower reduced order POD-BT/ROM was investigated. And then we proposed an state-space aeroservoelastic model and an active flutter control law design method based on the improved POD-BT/ROM.

2 POD-BT/ROM of aeroelastic systems

2.1 Dynamic linearization of the aeroelastic equation

By supposing that w is the conservative flow variable, $\mathbf{F}$ is the flux, $\mathbf{A}$ is the volume of the fluid cell, $\mathbf{u}$ is the structural general displacement and $\mathbf{v}$ is the structural general velocity, the aeroelastic system based on Euler/Navier-Stokes equation discretized by the finite volume method is written as follows [23]:

$$\left(\mathbf{A}(\mathbf{u})\mathbf{w}\right)_{,t} + \mathbf{F}(\mathbf{w}, \mathbf{u}, \mathbf{v}) = 0 \tag{1}$$

$$\mathbf{M}\mathbf{v}_{,t} + \mathbf{f}^{\text{int}}(\mathbf{u}, \mathbf{v}) = \mathbf{f}^{\text{ext}}(\mathbf{u}, \mathbf{w}) \tag{2}$$

where $\mathbf{M}$ is the mass matrix, $\mathbf{f}^{\text{int}}$ is the structural inner force, and $\mathbf{f}^{\text{ext}}$ is the aerodynamic load acting on structures. Supposing that $\Delta\mathbf{w}, \Delta\mathbf{u}, \Delta\dot{\mathbf{u}}$ are small perturbations around the steady state variables

$(\mathbf{w}_0, \mathbf{u}_0, \dot{\mathbf{u}}_0)$, we can obtain the following dynamic linearized equation:

$$\mathbf{A}_0\mathbf{w}_{,t} + \mathbf{H}\mathbf{w} + (\mathbf{E}+\mathbf{C})\mathbf{v} + \mathbf{G}\mathbf{u} = \mathbf{0} \tag{3}$$

$$\begin{aligned}
\mathbf{H} &= \frac{\partial \mathbf{F}}{\partial \mathbf{w}}(\mathbf{w}_0, \mathbf{u}_0, \mathbf{v}_0) \\
\mathbf{G} &= \frac{\partial \mathbf{F}}{\partial \mathbf{u}}(\mathbf{w}_0, \mathbf{u}_0, \mathbf{v}_0) \\
\mathbf{E} &= \frac{\partial \mathbf{A}}{\partial \mathbf{u}}\mathbf{w}_0 \\
\mathbf{C} &= \frac{\partial \mathbf{F}}{\partial \mathbf{v}}(\mathbf{w}_0, \mathbf{u}_0, \mathbf{v}_0)
\end{aligned} \tag{4}$$

where $\mathbf{A}_0$ is the volume of the fluid cell. To simplify the notation of the linearized equation, $\mathbf{w}$, $\mathbf{u}$, $\mathbf{v}$ are used to represent the perturbation variables $\Delta\mathbf{w}$, $\Delta\mathbf{u}$, $\Delta\mathbf{u}$, respectively. If the grid number of the CFD model is n, the order of Eq. (1) will be $J = 4n$ for two-dimensional problems, and $J = 5n$ for three-dimensional problems.

By letting:

$$\frac{1}{2}\rho_\infty V_\infty^2 \mathbf{P} = \frac{\partial \mathbf{f}^{\text{ext}}}{\partial \mathbf{w}}, \qquad \bar{\mathbf{K}}_S = \bar{\mathbf{K}} - \frac{\partial \mathbf{f}^{\text{ext}}}{\partial \mathbf{u}}(\mathbf{u}_0, \mathbf{w}_0) \tag{5}$$

the above dynamic linearization of the aeroelastic equation is arranged as:

$$\begin{bmatrix} \dot{\mathbf{w}} \\ \dot{\mathbf{v}} \\ \dot{\mathbf{u}} \end{bmatrix} = \begin{bmatrix} -\mathbf{A}_0^{-1}\mathbf{H} & -\mathbf{A}_0^{-1}(\mathbf{E}+\mathbf{C}) & -\mathbf{A}_0^{-1}\mathbf{G} \\ \frac{1}{2}\rho_\infty \mathbf{V}_\infty^2 \bar{\mathbf{M}}^{-1}\mathbf{P} & -\bar{\mathbf{M}}^{-1}\bar{\mathbf{C}} & -\bar{\mathbf{M}}^{-1}\bar{\mathbf{K}}_S \\ \mathbf{0} & \mathbf{I} & \mathbf{0} \end{bmatrix} \begin{bmatrix} \mathbf{w} \\ \mathbf{v} \\ \mathbf{u} \end{bmatrix} \tag{6}$$

Equation (6) is then transformed into the state space equation:

$$\begin{cases} \dot{\mathbf{w}} = \mathbf{A}\mathbf{w} + \mathbf{B}\mathbf{y} \\ \mathbf{F} = \mathbf{P}\mathbf{w} \end{cases} \tag{7}$$

where $\mathbf{A} = -\mathbf{A}_0^{-1}\mathbf{H}$, $\mathbf{B} = -\mathbf{A}_0^{-1}(\mathbf{E}+\mathbf{C}\ \ \mathbf{G})$, $\mathbf{y} = [\mathbf{v}\ \ \mathbf{u}]^T$. Equation (7) can be calculated in the time-domain or in the frequency-domain. In the time-domain, by applying the central differential scheme to Eq. (7), we obtain the snapshot equation:

$$\frac{\mathbf{w}^{n+1} - \mathbf{w}^n}{\Delta t} = \mathbf{A}\frac{\mathbf{w}^{n+1} + \mathbf{w}^n}{2} + \mathbf{B}\mathbf{y}^{n+1/2} \tag{8}$$

Then it is rearranged as follows;

$$\left(\mathbf{I} - \frac{\mathbf{A}\Delta t}{2}\right)\mathbf{w}^{n+1} = \left(\mathbf{I} + \frac{\mathbf{A}\Delta t}{2}\right)\mathbf{w}^n + \mathbf{B}\Delta t\mathbf{y}^{n+1/2} \tag{9}$$

The time responses or snapshots can be calculated from Eq. (9) by using the implicit time-marching method. For a real aeroelastic system, the input signals are always selected as the structural movements. Our POD/ROM solver used the Dirac triangle impulse function for every structural modal displacement and velocity.

For a three-dimensional aeroelastic system, if the order of the structural mode is s, the number of the meshes is n; consequently, the order of the aeroelastic system (6) is $J = 5n + 2s$. For a large mount of meshes, it is obvious that the direct computation of Eq. (9) is too expensive for the near real time simulation. It is also impractical for controller design because of the large order of Eq. (9). Therefore, the POD approach is used to reduce the full-order aeroelastic system.

2.2 Snapshot POD/ROM method

For one series of data $\{\mathbf{x}^k\}$, $\mathbf{x}^k \in \mathbf{C}^n$ in the n-dimensional space, the POD method searches an m-dimensional proper orthogonal subspace $\boldsymbol{\Psi} \in \mathbf{R}^{n\times m}$ to minimize the mapping errors from $\{\mathbf{x}^k\}$ to $\boldsymbol{\Psi}$ [38], where:

$$\begin{aligned}
\mathbf{G} &= \min_{\boldsymbol{\Phi}} \sum_{k=1}^{m} \left\| \mathbf{x}^k - \boldsymbol{\Phi}\boldsymbol{\Phi}^H\mathbf{x}^k \right\| \\
&= \sum_{k=1}^{m} \left\| \mathbf{x}^k - \boldsymbol{\Psi}\boldsymbol{\Psi}^H\mathbf{x}^k \right\|, \quad \boldsymbol{\Phi}^H\boldsymbol{\Phi} = \mathbf{I}
\end{aligned} \tag{10}$$

Equation (10) is equivalent to:

$$\begin{aligned}
\mathbf{H} &= \max_{\boldsymbol{\Phi}} \sum_{k=1}^{m} \frac{\langle (\mathbf{x}^k, \boldsymbol{\Phi})^2 \rangle}{\|\boldsymbol{\Phi}\|^2} \\
&= \sum_{k=1}^{m} \frac{\langle (\mathbf{x}^k, \boldsymbol{\Psi})^2 \rangle}{\|\boldsymbol{\Psi}\|^2}, \quad \boldsymbol{\Phi}^H\boldsymbol{\Phi} = \mathbf{I}
\end{aligned} \tag{11}$$

If the snapshot matrix $\{\mathbf{x}^k\}$, i.e., the time responses of unsteady aerodynamic loads, is calculated by numerical aeroelastic solvers to the Dirac function input signals, the mean value operator $\langle\cdot\rangle$ can be neglected. The constraint optimization problem of Eq. (11) is then transformed into the Lagrange equation:

$$J(\boldsymbol{\Phi}) = \sum_{k=1}^{m} \left(\mathbf{x}^k, \boldsymbol{\Phi}\right)^2 - \lambda\left(\|\boldsymbol{\Phi}\| - 1\right) \tag{12}$$

By solving the partial derivative objective function $J(\boldsymbol{\Phi})$ with respect to $\boldsymbol{\Phi}$, there is:

$$\frac{d}{d\boldsymbol{\Phi}} J(\boldsymbol{\Phi}) = 2\mathbf{X}\mathbf{X}^H\boldsymbol{\Phi} - 2\boldsymbol{\lambda}\boldsymbol{\Phi} \tag{13}$$

where $\mathbf{X} = \{\mathbf{x}^1, \ldots, \mathbf{x}^m\}$ is the matrix of snapshots. Equation (13) is set equal to zero, thus:

$$\left(\mathbf{X}\mathbf{X}^H - \lambda\mathbf{I}\right)\boldsymbol{\Psi} = 0 \tag{14}$$

Equation (14) is an real symmetry eigenvalue problem of the POD kernel $\mathbf{K} = \mathbf{X}\mathbf{X}^H$. For high order $\mathbf{K} \in \Re^{n\times n}$, the large eigenvalue problem is very difficult to solve. Because $\mathbf{X}\mathbf{X}^H$ and $\mathbf{X}^H\mathbf{X}$ have the same eigenvalues, $\boldsymbol{\Psi}$ can also be calculated from the follow lower m-dimensional problem:

$$\begin{cases} \mathbf{X}^{\mathrm{H}}\mathbf{X}\mathbf{V} = \mathbf{V}\boldsymbol{\Lambda} \\ \boldsymbol{\Psi} = \mathbf{X}\mathbf{V}\boldsymbol{\Lambda}^{-1/2} \end{cases} \tag{15}$$

where $\boldsymbol{\Psi} = [\psi_1\ \psi_2\ \ldots\ \psi_m]$, $\boldsymbol{\Lambda} = \mathrm{diag}(\lambda_1\ \lambda_2\ \ldots\ \lambda_m)$, and $\lambda_1 \geq \lambda_2 \geq \cdots \geq \lambda_m$. By truncating $\boldsymbol{\Psi}$ to the r-order vector $\boldsymbol{\Psi}_r = [\psi_1\ \psi_2\ \ldots\ \psi_r]$, the full-order series $\mathbf{x}^{n\times 1}$ can be reduced to an r-order system:

$$\mathbf{x}^{n\times 1} = \boldsymbol{\Psi}_r\boldsymbol{\xi}^{r\times 1} \tag{16}$$

Then, by projecting the full-order equation (7) into $\boldsymbol{\Psi}_r$, we can obtain the reduced fluid model:

$$\begin{cases} \dot{\mathbf{w}}_r = \boldsymbol{\Psi}_r^T\mathbf{A}\boldsymbol{\Psi}_r\mathbf{w}_r + \boldsymbol{\Psi}_r^T\mathbf{B}\mathbf{y} \\ \mathbf{F} = \mathbf{P}\boldsymbol{\Psi}_r\mathbf{w}_r \end{cases} \tag{17}$$

Finally, by substituting Eq. (17) into Eq. (6), the traditional r-order time-domain POD/ROM of the aeroelastic system can be represented as follows:

$$\begin{bmatrix} \dot{\mathbf{w}}_r \\ \dot{\mathbf{v}} \\ \dot{\mathbf{u}} \end{bmatrix} = \begin{bmatrix} -\boldsymbol{\Psi}_r^T\mathbf{A}_0^{-1}\mathbf{H}\boldsymbol{\Psi}_r & -\boldsymbol{\Psi}_r^T\mathbf{A}_0^{-1}(\mathbf{E}+\mathbf{C}) & -\boldsymbol{\Psi}_r^T\mathbf{A}_0^{-1}\mathbf{G} \\ \frac{1}{2}\rho_\infty\mathbf{V}_\infty^2\bar{\mathbf{M}}^{-1}\mathbf{P}\boldsymbol{\Psi}_r & -\bar{\mathbf{M}}^{-1}\bar{\mathbf{C}} & -\bar{\mathbf{M}}^{-1}\bar{\mathbf{K}}_S \\ \mathbf{0} & \mathbf{I} & \mathbf{0} \end{bmatrix} \begin{bmatrix} \mathbf{w}_r \\ \mathbf{v} \\ \mathbf{u} \end{bmatrix} \tag{18}$$

The order of the reduced system in Eq. (18) is only $q = 2s + r$ and it is much smaller than that of the original system in Eq. (6). The POD/ROM is convenient for analyzing the stability and observing the time response of nonlinear aeroelastic systems, and it is much simpler and more efficient than the full-order CFD simulation.

2.3 POD-BT/ROM

For a very large scale three-dimensional aeroelastic system, the order of Eq. (18) is still larger than that of the expected model, especially for control law design. So that the balanced truncation method is applied to further reduce the traditional time-domain POD/ROM from hundreds to tens.

Equation (18) is transformed into the general state space equation:

$$\begin{cases} \dot{\mathbf{x}}_r = \mathbf{A}_r\mathbf{x}_r + \mathbf{B}_r\mathbf{u}_r \\ \mathbf{y}_r = \mathbf{C}_r\mathbf{x}_r \end{cases} \tag{19}$$

where $\mathbf{x}_r, \mathbf{u}_r, \mathbf{y}_r$ are the state variables, input variables, and output variables, respectively. The observability Gramian and controllability Gramian of Eq. (19) are:

$$\begin{cases} \mathbf{W}_c = \int_0^\infty \mathbf{e}^{A_r t}\mathbf{B}_r\mathbf{B}_r^T\mathbf{e}^{A_r^T t}\,dt \\ \mathbf{W}_o = \int_0^\infty \mathbf{e}^{A_r^T t}\mathbf{C}_r^T\mathbf{C}_r\mathbf{e}^{A_r t}\,dt \end{cases} \tag{20}$$

Integrating Eq. (20) in the frequency domain, produces:

$$\begin{cases} \mathbf{W}_c = \dfrac{1}{2p}\displaystyle\int_{-\infty}^{+\infty} (jw\mathbf{I}-\mathbf{A})^{-1}\mathbf{B}_r\mathbf{B}_r^T \\ \qquad \times \left(-jw\mathbf{I}-\mathbf{A}_r^T\right)^{-1} dw \\ \mathbf{W}_o = \dfrac{1}{2p}\displaystyle\int_{-\infty}^{+\infty} (-jw\mathbf{I}-\mathbf{A}_r^T)^{-1}\mathbf{C}_r^T\mathbf{C}_r \\ \qquad \times (jw\mathbf{I}-\mathbf{A}_r)^{-1} dw \end{cases} \tag{21}$$

With the transformation $\mathbf{x} = \mathbf{T}\hat{\mathbf{x}}$, the Gramian matrices can then be transformed to diagonal matrices, as follows:

$$\begin{cases} \hat{\mathbf{W}}_c = \mathbf{T}^{-1}\mathbf{W}_c\mathbf{T}^{-T} \\ \hat{\mathbf{W}}_o = \mathbf{T}^T\mathbf{W}_o\mathbf{T} \\ \hat{\mathbf{W}}_o = \hat{\mathbf{W}}_c = \boldsymbol{\Sigma} \end{cases} \tag{22}$$

where $\boldsymbol{\Sigma} = \mathrm{diag}(\sigma_1^2\ \sigma_2^2\ \ldots\ \sigma_n^2)$, and $\sigma_1 \geq \sigma_2 \geq \cdots \geq \sigma_n$ are the Hankel singular values. Supposing $\boldsymbol{\Sigma}_1 = \mathrm{diag}(\sigma_1^2\ \sigma_2^2\ \ldots\ \sigma_s^2)$, $\boldsymbol{\Sigma}_2 = \mathrm{diag}(\sigma_{s+1}^2\ \sigma_{s+2}^2\ \ldots\ \sigma_n^2)$, and only preserving the column vectors of the Gramian matrices relate to $\boldsymbol{\Sigma}_1$, the original high order equation (19) can be reduced to an new lower s-order system. The required reduced transformation matrices can be calculated by the following algorithm [37]:

(1) Firstly, calculate the Gramian matrices from Eq. (20) and Eq. (21).

(2) Then, decompose the Gramian matrices by the Choleski method, as follows:

$$\mathbf{W}_c = \mathbf{X}\mathbf{X}^T, \qquad \mathbf{W}_o = \mathbf{Z}\mathbf{Z}^T \tag{23}$$

(3) Thirdly, apply the singular value decomposition(SVD) to $\mathbf{Z}^T\mathbf{X}$:

$$\begin{aligned} \mathbf{Z}^T\mathbf{X} &= \mathbf{U}\boldsymbol{\Sigma}\mathbf{V}^T \\ &= \begin{bmatrix}\mathbf{U}_1 & \mathbf{U}_2\end{bmatrix}\begin{bmatrix}\boldsymbol{\Sigma}_1 & 0 \\ 0 & \boldsymbol{\Sigma}_2\end{bmatrix}\begin{bmatrix}\mathbf{V}_1^T \\ \mathbf{V}_2^T\end{bmatrix} \end{aligned} \tag{24}$$

(4) Finally, the transformation matrices $\mathbf{T}_s$ and $\mathbf{S}_s$ can be calculated as follows:

$$\mathbf{T}_s = \mathbf{X}\mathbf{V}_1\boldsymbol{\Sigma}_1^{-1/2}, \qquad \mathbf{S}_s = \boldsymbol{\Sigma}_1^{-1/2}\mathbf{U}_1^T\mathbf{Z}^T \tag{25}$$

Thus, the further reduced new s-order time-domain ROM, called POD-BT/ROM, can be constructed as follows:

$$\begin{cases} \dot{\mathbf{x}}_s = \mathbf{S}_s\mathbf{A}_r\mathbf{T}_s\mathbf{x}_r + \mathbf{S}_s\mathbf{B}_r\mathbf{u}_r \\ \mathbf{y}_s = \mathbf{C}_r\mathbf{T}_s\mathbf{x}_r \end{cases} \tag{26}$$

3 Simulation cases

3.1 NACA0012 aeroelastic system

3.1.1 Linearization model validation

The dynamic equation for NACA 0012 PAPA aeroelastic system is [33]:

$$\begin{aligned} &\begin{bmatrix}1 & x_\alpha \\ x_\alpha & r_\alpha^2\end{bmatrix}\begin{bmatrix}\ddot{\bar{h}} \\ \ddot{\alpha}\end{bmatrix} + \begin{bmatrix}(\omega_h/\omega_\alpha)^2 & 0 \\ 0 & r_\alpha^2\end{bmatrix}\begin{bmatrix}\bar{h} \\ \alpha\end{bmatrix} \\ &\quad = \frac{1}{\pi}V^{*2}\begin{bmatrix}-C_L \\ C_M\end{bmatrix} \end{aligned} \tag{27}$$

where h and α are the plunge and pitch angle freedoms of the system respectively, r_α is the radius of the gyration of the airfoil around elastic axis, x_α is the static dimensionless distance between the gravity center position and the hinge axis. ω_h and ω_α are the uncoupled natural frequency of the plunge and pitch movement. $V^* = U_\infty/(\omega_\alpha b\sqrt{\mu})$ is defined as the reduced velocity where $\mu = m/(\pi\rho_\infty b^2)$. The structural parameters are $x_\alpha = 1.8$, $r_\alpha^2 = 3.48$, $\alpha = -2.0$, $\mu = 60.0$, and $\omega_h/\omega_\alpha = 1$.

In order to accurately predict the aeroelastic responses, the unsteady aerodynamics, C_L and C_M, should be calculated by the coupled solver. The Euler equation is discretized by the second-order Van Leer scheme on the 100×40 O-type structure-based meshes. So that the order of the full-order linearized flow equation is $J = 4 \times 100 \times 40 = 40000$. The initial flow parameters are $Ma = 0.601$, $\rho_\infty = 1.225\ \mathrm{kg/m^3}$, $p_\infty = 101325$ Pa, and $\alpha = 0°$. The airfoil moves as $h = 0.01\sin(12.80236(t_i - 1)\cdot dt_i)$ and $\alpha = 0.02\sin(12.80236(t_i - 1)\cdot dt_i)$ simultaneously. Figure 1 plots the time responses of the unsteady aerodynamic loads at the time step 0.001 s, which are predicted by the dynamic linearization equation and the nonlinear CFD solver respectively. The good agreement of the two solvers indicates that in small perturbation the linearized model has nearly the same accuracy as the nonlinear CFD model.

3.1.2 POD-BT/ROM validation

The order of the dynamic linearized aeroelastic model is 40040. We reduced the full-order aeroelastic model to an 80-order POD/ROM and a 5-order POD-BT/ROM respectively. In the same flow condition as above, the

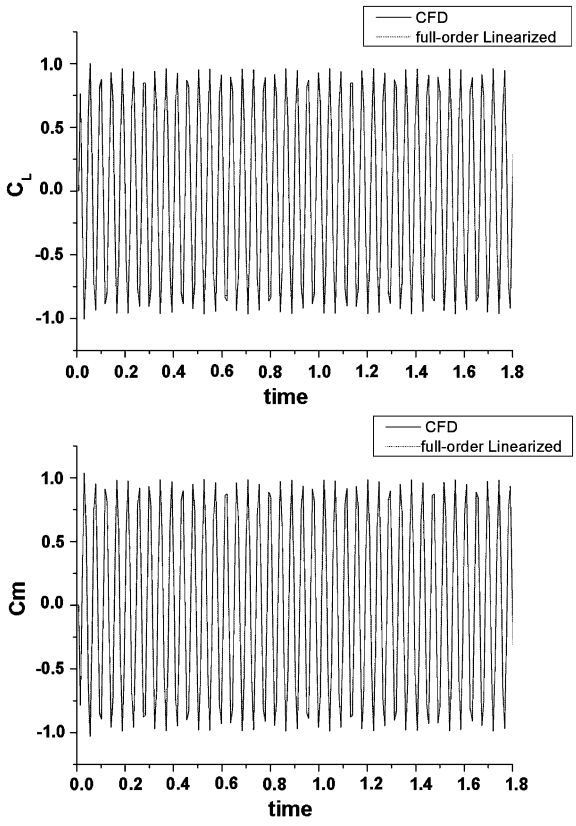

Fig. 1 The responses of the linearized model vs. nonlinear CFD solver

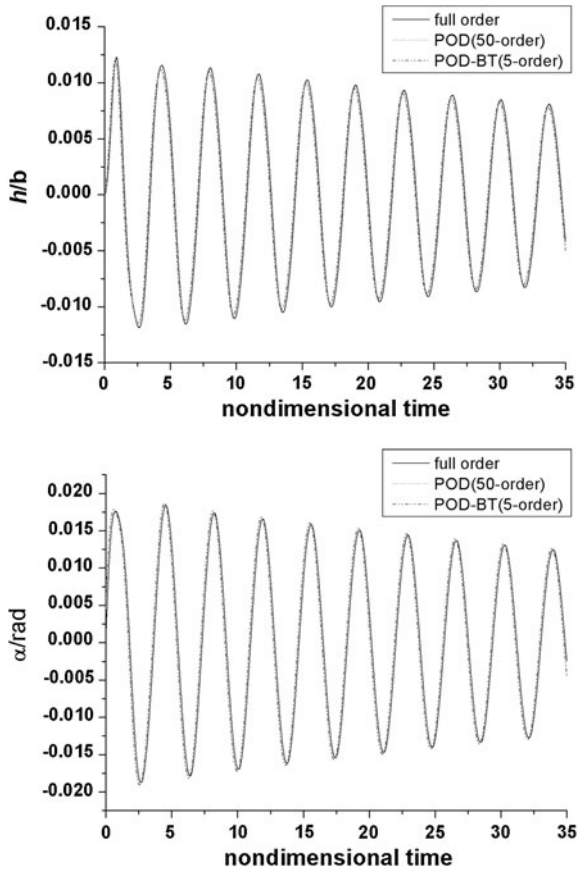

Fig. 2 The aeroelastic responses of different models

aeroelastic responses predicted by different models were presented in Fig. 2. It showed that the 5-order POD-BT/ROM nearly had the same accuracy as the 80-order time-domain POD/ROM and the full-order linearized model. For its good accuracy and lower order, the POD-BT/ROM would be an attractive model for the aeroservoelastic synthesis.

3.2 AGARD 445.6 wing

3.2.1 Aeroelastic responses: POD/ROM vs. POD-BT/ROM

In order to further validate the performance of the POD-BT/ROM, the three-dimensional AGARD 445.6 wing model was demonstrated. The degree-of-freedom of the full-order aeroelastic system is 239408, including the degree-of-freedoms of the first four structural modes. At the Mach number 0.678, the snapshots equation (9) was used to calculated the snapshots with the time step of 0.0001 s. The unsteady general aerodynamic coefficients of the first 200 time steps were selected to construct three different order POD/ROMs, including a 50-order, a 150-order ROM, and a 300-order ROM. At the Ma number 0.678 and the reduced speed 0.407, the responses of the first two structural modes predicted by the different POD/ROMs and the full-order linearization model were compared in Fig. 3. It shows that the 300-order POD/ROM has the enough accuracy as the full-order model. The CFD/CSD-coupled aeroelastic solver took approximately 6 hours to calculate the structural responses, while the POD/ROM only required approximately 2 minutes. Even when the cost of building the POD/ROM is accounted, the computational efficiency is nearly increased by an order of magnitude.

Although the order of the traditional time-domain POD/ROM is much small than that of the original full-order system(i.e., 240 K), the hundreds of order is still too large for some applications, i.e., active control law design. So that a 600-order time-

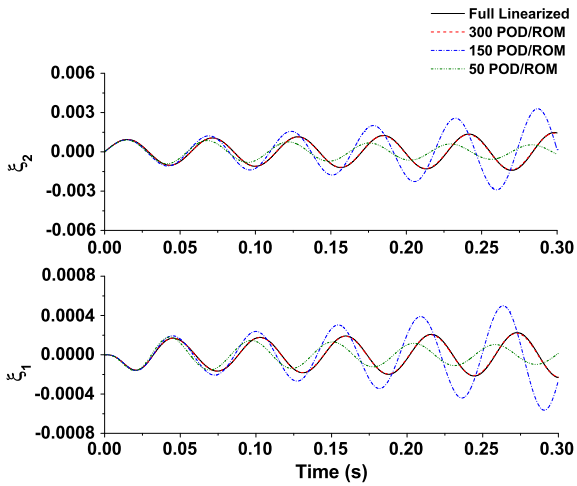

Fig. 3 POD/ROM vs. full-order at Mach 0.678

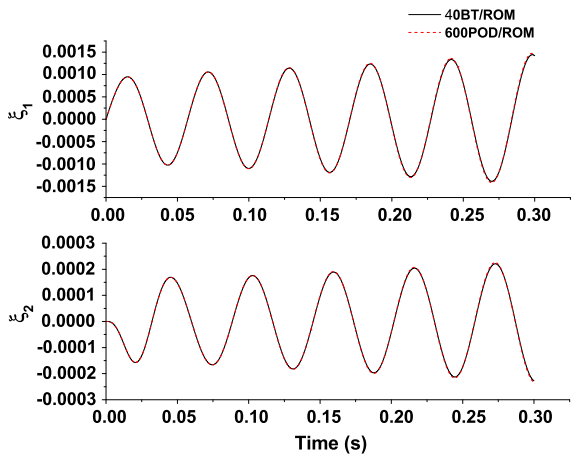

Fig. 4 40-order BT vs. 600-order POD at Mach 0.901

domain POD/ROM and a 40-order POD-BT/ROM were constructed at Mach 0.901. Figure 4 plots the general structural displacements predicted by the two ROMs under the reduced velocity $V^* = 0.3873$. The good agreement of the two results indicates that POD-BT/ROM overcomes the drawback that the order of the time-domain POD/ROM is higher than that of the frequency-domain POD/ROM.

3.2.2 Flutter boundary prediction

After constructing a ROM for an aeroelastic system at an given Mach number, we can obtain a series of system matrices by changing the dynamic pressures at the given Mach number. And then the flutter velocity and flutter frequency at the given Mach number can be predicted very quickly, just by analyzing the eigenvalues of these system matrices. Repeating the same procedure in different Mach number, the flutter boundary can then be obtained quickly. Figure 5 plots the flutter boundaries predicted by the 40-order POD-BT/ROM, the 300-order POD/ROM, and the CFD/CSD coupled aeroelastic solver. The agreement of the curves indicated again that the POD-BT/ROM has good accuracy as the coupled aeroelastic solver and the traditional time-domain POD/ROM.

4 Active control law design method based on POD-BT/ ROM

4.1 Aeroelastic and aeroservoelastic state equation

The aeroservoelastic dynamic equation is dependent on the type of the actuators. As a demonstration, only one flap control surface is used to stabilize the aeroelastic system in the rear-edge of the wing structure. By adding the unsteady aerodynamic perturbation of the flap control to the POD/BT-ROM aeroelastic model in Eq. (26), the reduced order aeroservoelastic state equation is obtained as:

$$\begin{bmatrix} \dot{\mathbf{w}}_r \\ \dot{\mathbf{v}} \\ \dot{\mathbf{u}} \end{bmatrix} = \begin{bmatrix} -\boldsymbol{\Psi}_r^T \mathbf{A}_0^{-1} \mathbf{H} \boldsymbol{\Psi}_r & -\boldsymbol{\Psi}_r^T \mathbf{A}_0^{-1} (\mathbf{E} + \mathbf{C}) & -\boldsymbol{\Psi}_r^T \mathbf{A}_0^{-1} \mathbf{G} \\ \frac{1}{2} \rho_\infty \mathbf{V}_\infty^2 \bar{\mathbf{M}}^{-1} \mathbf{P}_w \boldsymbol{\Psi}_r & -\bar{\mathbf{M}}^{-1} \bar{\mathbf{C}} & -\bar{\mathbf{M}}^{-1} \bar{\mathbf{K}}_S \\ \mathbf{0} & \mathbf{I} & \mathbf{0} \end{bmatrix} \begin{bmatrix} \mathbf{w}_r \\ \mathbf{v} \\ \mathbf{u} \end{bmatrix} + \mathbf{q}_\infty \begin{bmatrix} \mathbf{P}_{w\beta} \\ \mathbf{P}_{f\beta} \\ \mathbf{0} \end{bmatrix} \boldsymbol{\beta} \tag{28}$$

where the $\boldsymbol{\beta}$ is the deflection of the flap, $\mathbf{P}_{w\beta}$ is the perturbation matrix of the unit deflection of the flap to the flow field variables, and $\mathbf{P}_{f\beta}$ is the perturbation matrix of the unit deflection of the flap to the general aerodynamic force. All of these control matrices can be precomputed by the CFD solver and then projected on the

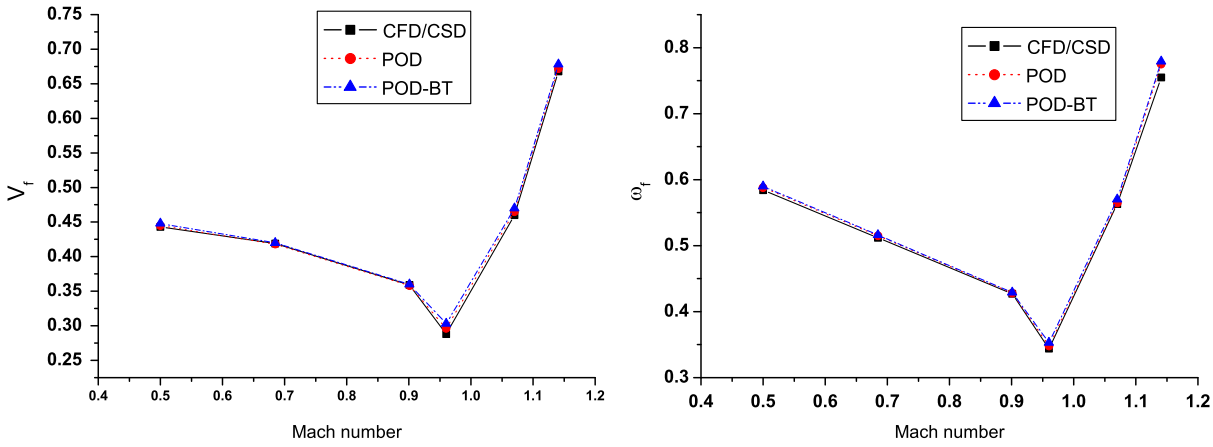

Fig. 5 Flutter boundary of AGARD wing(POD/ROM vs. CFD/CSD)

POD basis at the given Mach number. Thus, the control plant model of the aeroelastic system is rewritten as follows:

$$\begin{cases} \dot{\mathbf{x}} = \mathbf{A}(q_\infty)\mathbf{x} + \mathbf{B}(q_\infty)\boldsymbol{\beta} \\ \mathbf{y} = \mathbf{C}\mathbf{x} \end{cases} \tag{29}$$

The state variables are the reduced flow parameters and structural movement variables, the input of the aeroservoelastic system (29) is the deflection of the control surface $\boldsymbol{\beta}$, and the output variable $\mathbf{y}$ is the structural responses, i.e., the displacement and velocity. The objective of the active control law design problem is to find a control law $\boldsymbol{\beta} = -\mathbf{K}(\mathbf{y})$ to stabilize the unstable system responses. In general, for the case of multiple control surfaces, the POD-BT/ROM based aeroservoelastic model is the same as Eq. (29), if more control matrices is calculated and added. In this case, the control matrix $\mathbf{B}$ will become a multi-dimensional matrix.

4.2 Active flutter suppression of the Goland wing+ model

4.2.1 The Goland+ wing model

The Goland+ wing model is developed as a transonic flutter test case by Eastep and Olsen [39]. The configuration of the Goland+ wing is presented in Fig. 6, where the flap control surface located in the middle of the rear edge area. About 0.4 million of fluid meshes was used for the CFD/CSD solver. The infinite plate spline method was used to deal with the mesh mapping between the fluid and structure.The spring analogy dynamic mesh algorithm was applied to update the movement of the computational grids. At Mach 0.82 and zero angle of attack, a 40-order POD-BT /ROM was constructed and validated. Then the POD/BT-ROM was applied to search the flutter point at Mach 0.82 with the time step of 0.001 s, where the initial perturbation velocity 0.1 was given to the second structural mode. At dynamic pressure 24787, the system will run into flutter as indicated in Fig. 6. It took only several minutes for the ROM to find the flutter point f, while nearly twenty hours were used for the CFD/CSD couple solver to obtain the similar result.

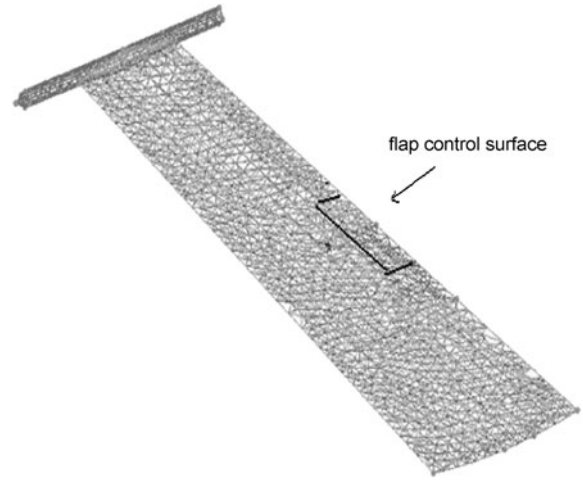

Fig. 6 Configuration of Goland +wing model

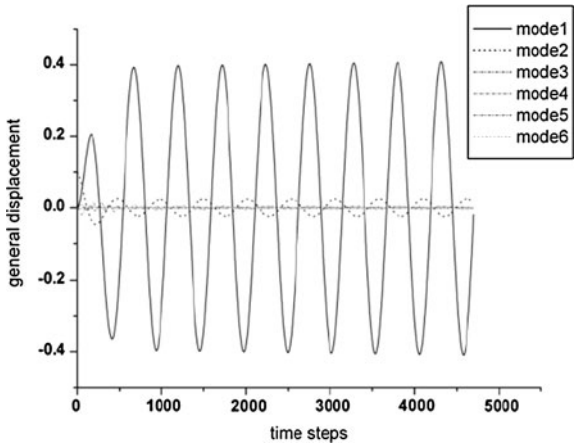

Fig. 7 The flutter of the wing at $a = 0.82$, $q = 24787$

4.2.2 *Optimal static output feedback controller design method*

In most of the practical aeroelastic control problems, it is impossible to measure all the state variables of the system. So the classic LQR controller and many adaptive state feedback controllers require at least one state observer to estimate these state variables. However, the observer will reduce the robustness of the controller. Meanwhile, the real-time implementation of high-order controllers is also quite problematic. Unlike many state feedback controllers (i.e., LQR and LQG controller), the optimal static output feedback (SOF) controller with constant control gains, is based on the direct feedback of the sensors' output [40]. The SOF design method does not assume the availability of all the system state variables for feedback. It is assumed that only a few linear combinations of system states can be directly measured from the sensors. For example, the nonlinear aerodynamics cannot be directly measured and feed-backed. So that SQF method is very suitable for the active control law design based on the aeroelastic ROM. Actually SQF controller had been successfully applied to flutter suppression of a wing [36] and a full aircraft [41].

An optimal SOF controller aims to find the feedback gains that optimize the given performance index. For an nth-order LTI stabilizable system:

$$\begin{cases} \dot{\mathbf{x}} = \tilde{\mathbf{A}}\mathbf{x} + \tilde{\mathbf{B}}\mathbf{u} + \tilde{\mathbf{D}}\mathbf{w} \\ \mathbf{y} = \tilde{\mathbf{C}}\mathbf{x} \end{cases} \tag{30}$$

where $\mathbf{x}$ is the system state variable, $\tilde{\mathbf{A}}$ is the system dynamic matrix in state-space form, $\mathbf{u}$ is the command of the actuator, $\tilde{\mathbf{B}}$ is the control matrix, $\mathbf{y}$ is the measurement of the sensors, $\tilde{\mathbf{C}}$ is the matrix relating the sensor's measurements to the state variables, $\mathbf{w}$ is the zero-mean unit intensity white noise process, and $\tilde{\mathbf{D}}$ is the matrix of noise intensity. Suppose the constant-gain output feedback control law as the form:

$$\mathbf{u}(t) = -\mathbf{K}\mathbf{y}(t) \tag{31}$$

where the feedback gains $\mathbf{K}$ is selected such that it can stabilizes the closed-loop system and minimize the quadratic performance measurement:

$$J = \frac{1}{2}\int_0^\infty \left[\mathbf{x}^T(t)\mathbf{Q}\mathbf{x}(t) + \mathbf{u}^T(t)\mathbf{R}\mathbf{u}(t)\right] dt \tag{32}$$

The solution of the above optimization problem is:

$$\begin{aligned} &\mathbf{K} = \mathbf{R}^{-1}\tilde{\mathbf{B}}\mathbf{P} \\ &\mathbf{P}\tilde{\mathbf{A}} + \tilde{\mathbf{A}}^T\mathbf{P} - \mathbf{P}\tilde{\mathbf{B}}\mathbf{R}^{-1}\tilde{\mathbf{B}}^T\mathbf{P} + \mathbf{Q} = \mathbf{0} \end{aligned} \tag{33}$$

where $\mathbf{P}$ is the solution of the Riccati equation, which can be calculated by many iterative algorithms [40].

Four outputs are used, including the twist sensors, curvature sensors, the corresponding twist-rate and curvature-rate sensors. The velocity of the structural modes can be identified from the outputs of the sensors. As a demonstration, the sensors are ideal sensors without errors and delays. From the simulation results as Fig. 7, it is found that the amplitudes of the mode 1 and mode 2 are the largest. It implies that the aeroelastic system is dominated by the torsion and bending deformations. So we just identify the output information of the first two structural modes from the sensors, thus, the SOF controller can be reduced to a second-order controller. The control law is now selected as $\delta = [K_1 \;\; K_2][\dot{\xi}_1 \;\; \dot{\xi}_2]^T$. After determinating the structure of the SOF controller, the optimal control gain $\mathbf{K} = [0.01, 0.001]$ was selected by the MATLAB/SIMULINK with $\mathbf{Q} = \mathbf{0}$ and $\mathbf{P} = \mathbf{I}$, according to the SQF algorithm.

4.2.3 *Flutter suppression simulation with SQF controller*

The POD-BT/ROM and CFD/CSD coupled aeroelastic solver were both used to simulate the flutter suppression under dynamic pressure 29498.6 Pa and Mach 0.82 with the time-step size of 0.001 s. Figure 8 plots the aeroelastic responses of the structure

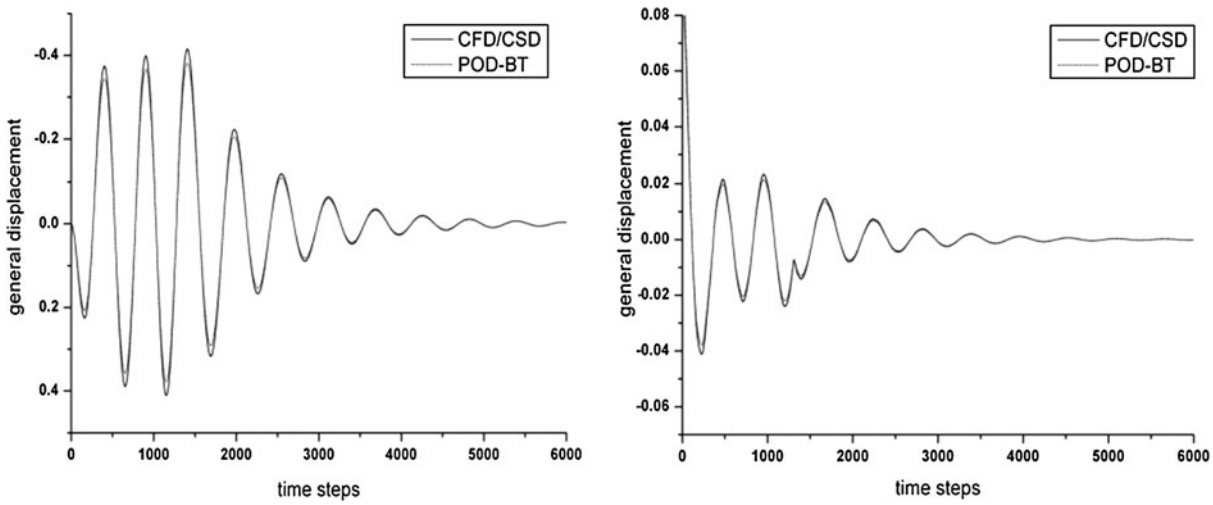

Fig. 8 Comparison of the structural responses of ROM vs. CFD/CSD solver with controller

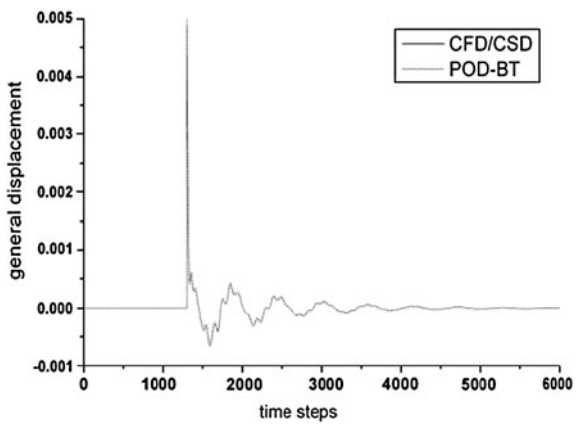

Fig. 9 Comparison of the response of the control surface

and Fig. 9 shows the control command of the control surface. The wing/store aeroelastic system diverges very quickly at the initial time steps. However, after the SQF controller start from the 1300th time step, the unstable response is suppressed very quickly. The responses of the ROM and the coupled solver also agree well.

The robustness of the controller is a very important, because it's impossible to build an absolutely accurate control plant model, and the model errors always exist. The other reason is that the properties of the structure have uncertainties during flight, such as the separation of the wing-tip store. Consequently, an analysis of the robustness of the active controller is required. By allowing the structural stiffness to reduce by 20 %, the time responses of the aeroelastic system are calculated by the CFD/CSD couple solver under the same condition as the above. The simulation results plotted in Fig. 10 show that the SQF controller designed based on the POD-BT/ROM can still suppress the unstable system quickly.

5 Conclusion

A POD-BT/ROM were investigated by incorporating the balanced truncation procedure in the framework of the traditional time-domain POD/ROM. The validation cases show that the several tens-order POD-BT/ROM nearly has the same accuracy as the several hundreds-order time-domain POD/ROM. It enables the time-domain POD/ROM to have the same accuracy as the frequency-domain POD/ROM at the same low order. The active flutter suppression control law design method based on the POD-BT/ROM was proposed and demonstrated by the Goland wing+/store system. If the control matrix is calculated in the frequency domain, the framework of the control law design is very similar for the frequency-domain POD/ROM. In the further research, the proposed method will be applied to more complex aeroelastic system, such as full flexible aircrafts, MIMO aeroelastic systems with multiple control surfaces.

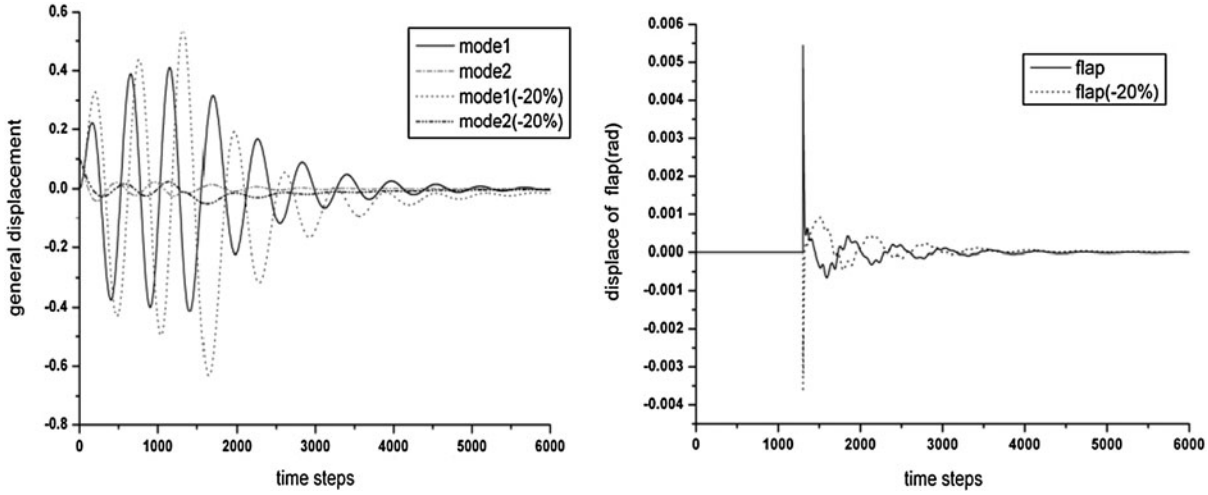

Fig. 10 The structural and flap response of CFD/CSD solver with the controller

Acknowledgements The work was partially supported by the National Natural Science Foundation of China (10902082, 91016008), New Faculty Research Foundation of XJTU, and the Funds for the Central Universities (xjj20100126).

References

1. Mukhopadhyay, V.: Historical perspective on analysis and control of aeroelastic responses. J. Guid. Control Dyn. **26**(5), 673–684 (2003)
2. Allen, C.B., Fenwick, C.L., Taylor, N.V., Djayapertapa, L.: Investigation of flutter suppression by active control. AIAA 2003-3510 (2003)
3. Zhang, R., Singh, S.N.: Adaptive output feedback control of an aeroelastic system with unstructured uncertainties. J. Guid. Control Dyn. **24**(3), 502–509 (2001)
4. Platanitis, G., Strganac, T.W.: Control of a nonlinear wing section using leading- and trailing-edge surfaces. J. Guid. Control Dyn. **27**(1), 52–58 (2004)
5. Zebb, P., Ben, C., Con, D., Strganac, T.W.: Linear-parameter-varying control of an improved three-degree-of-freedom aeroelastic model. J. Guid. Control Dyn. **33**(2), 615–618 (2010)
6. Chen, G., Sun, J., Zuo, Y., Li, Y.M.: Linear parameter varying control for active flutter suppression based on adaptive reduced order model. AIAA 2011-1773 (2011)
7. ZONA Technology, Inc.: ZAERO User's Manual. Ver. 7.3. Scottsdale, AZ, October 2005
8. Boldelli, D.H., Chen, P.C., Panza, J., Adams, J.: Unified rational function approximation formulation for aeroelastic and flight dynamics analyses. AIAA paper 2006-2025 (2006)
9. Lucia, D.J., Beran, P.S., Silva, W.A.: Reduced-order modeling: new approaches for computational physics. Prog. Aerosp. Sci. **40**(1), 51–117 (2004)
10. Dowell, E.H.: Some recent advances in nonlinear aeroelasticity: fluid-structure interaction in the 21st century. AIAA-2010-3137 (2010)
11. Badcock, K.J., Timme, S., Marques, S., Khodaparast, H., Prandina, M., Mottershead, J.E., Swift, A., Da Ronch, A., Woodgate, M.A.: Transonic aeroelastic simulation for instability searches and uncertainty analysis. Prog. Aerosp. Sci. **47**, 392–423 (2011)
12. Lucia, D.J., Beran, P.S., Silva, W.A.: Reduced-order modeling: new approaches for computational physics. Prog. Aerosp. Sci. **40**(1), 51–117 (2004)
13. Silva, W.A., Bartels, R.E.: Development of reduced-order models for aeroelastic analysis and flutter prediction using the CFL3Dv6.0 code. J. Fluids Struct. **19**(6), 729–745 (2004)
14. Cowan, T.J., Andrew, S.A.J., Gupta, K.K.: Accelerating computational fluid dynamics based aeroelastic predictions using system identification. J. Aircr. **38**(1), 81–87 (2001)
15. Woodgate, M.A., Badcock, K.J.: Fast prediction of transonic aeroelastic stability and limit cycles. AIAA J. **45**(6), 1370–1381 (2007)
16. Chen, G., Li, Y.M., Yan, G.R.: A nonlinear POD reduced order model for limit cycle oscillation prediction. Sci. China Ser. G **53**(6), 1325–1332 (2010)
17. Romannowski, M.C., Dowell, E.H.: Reduced order unsteady aerodynamic and aeroelastic models using Karhunen-Loéve eigenmodes. In: 6th AIAA/USAF/NASA/ISSMO Symposium on Multidisciplinary Analysis and Optimization, Atlanta, GA, pp. 7–13 (1996)
18. Hall, K.C., Thomas, J.P., Dowell, E.H.: Proper orthogonal decomposition technique for transonic unsteady aerodynamic flows. AIAA J. **38**(2), 1853–1862 (2000)
19. Thomas, J.P., Dowell, E.H., Hall, K.C.: Three-dimensional transonic aeroelasticity using proper orthogonal decomposition based reduced order models. J. Aircr. **40**(3), 544–551 (2003)
20. Thomas, J.P., Dowell, E.H., Hall, K.C.: Virtual aeroelastic flight testing for the F-16 fighter with stores. AIAA-2007-1640 (2007)

21. Henshawa, M.J., Badcock, K.J., Vio, G.A.: Non-linear aeroelastic prediction for aircraft applications. Prog. Aerosp. Sci. **434**(4–6), 65–137 (2007)
22. Falkiewicz, N.J., Cesnik, C.E.S.: Proper orthogonal decomposition for reduced-order thermal solution in hypersonic aerothermoelastic simulations. AIAA-2010-2798 (2010)
23. Lieu, T., Farhat, C.: Adaptation of aeroelastic reduced-order models and application to an F-16 configuration. AIAA J. **45**(6), 1244–1257 (2007)
24. Woodgate, M.A., Badcock, K.J.: Implicit harmonic balance solver for transonic flow with forced motions. AIAA J. **47**(4), 893–901 (2009)
25. Thomas, J.P., Dowell, E.H., Hall, K.C.: Using automatic differentiation to create a nonlinear reduced order model aeroelastic solver. AIAA J. **48**(1), 19–24 (2010)
26. Chen, G., Li, Y., Yan, G.-R.: Limit cycle oscillation prediction and control design method for aeroelastic system based on new nonlinear reduced order model. Int. J. Comput. Methods **8**(1), 77–90 (2011)
27. Chen, G., Li, Y.M., Yan, G.R.: A fast aeroelastic response prediction method based on proper orthogonal decomposition reduced order. Model. J. Astronaut. **30**(5), 1765–1769 (2009) (In Chinese)
28. Farhat, C., Amsallem, D.: Recent advances in reduced-order modeling and application to nonlinear computational aeroelasticity. AIAA-2008-562 (2008)
29. Beran, P.S., Lucia, D.J., Pettit, C.L.: Reduced-order modelling of limit-cycle oscillation for aeroelastic systems. J. Fluids Struct. **19**, 575–590 (2004)
30. Pettit, C.L., Beran, P.S.: Application of proper orthogonal decomposition to the discrete Euler equations. Int. J. Numer. Methods Eng. **55**(4), 479–497 (2002)
31. Danowsky, B.P., Peter, M.T., Farhat, C., Lieu, T., Harris, C., Lechniak, J.: Incorporation of feedback control into a high-fidelity aeroservoelastic fighter aircraft model. J. Aircr. **47**(4), 1274–1282 (2010)
32. Hu, P., Bodson, M., Brenner, M.: Towards real-time simulation of aeroservoelastic dynamics for a flight vehicle from subsonic to hypersonic regime. AIAA-2008-6375 (2008)
33. Falkiewicz, N.J., Cesnik, C.E.S., Crowell, A.R., McNamara, J.J.: Reduced-order aerothermoelastic framework for hypersonic vehicle control simulation. AIAA J. **49**(8), 1625–1646 (2011)
34. Marzoeea, P., Silva, W.A., Libreseu, L.: Open/closed-loop nonlinear aeroelasticity for airfoils via Volterra series approach. AIAA J. **42**(4), 673 (2004)
35. Zhang, Z.J., Min, X., Chen, S.L.: Active flutter control of transonic flapped wing based on CFD/CSD coupling. In: 7th International Conference on System Simulation and Scientific Computing (ICSC'2008), Beijing, China, p. 430 (2008)
36. Chen, G., Li, Y.M., Yan, G.R.: Active control stability/augmentation system design based on reduced order model. Chin. J. Aeronaut. **23**(6), 637–644 (2010)
37. Moore, B.C.: Principal component analysis in linear system: controllability, observability, and model reduction. IEEE Trans. Autom. Control **26**(1), 17–31 (1981)
38. Holmes, P., Lumley, J.L., Berkooz, G.: Turbulence, Coherent Structures, Dynamical Systems and Symmetry. Cambridge University Press, Cambridge (1996)
39. Eastep, F.E., Olsen, J.J.: Transonic flutter analysis of a rectangular wing with conventional airfoil sections. AIAA J. **18**(10), 1159–1164 (1980)
40. Syrmos, V.L., Abdallah, C.T., Dorato, P., Grigoriadis, K.: Static output feedback: a survey. Automatica **33**(2), 125–137 (1997)
41. Patil, M.J., Hodges, D.H.: Output feedback control of the nonlinear aeroelastic response of a slender wing. J. Guid. Control Dyn. **25**(2), 302–308 (2002)